

Estimation of the Mutual Orientation and Intermolecular Interaction of $C_{12}E_x$ from Molecular Dynamics Simulations

Maria Velinova, Yana Tsoneva, Anela Ivanova, and Alia Tadjer*

Laboratory of Quantum and Computational Chemistry, Department of Physical Chemistry, Faculty of Chemistry and Pharmacy, University of Sofia, 1 James Bourchier Avenue, 1164 Sofia, Bulgaria

S Supporting Information

ABSTRACT: Nonionic surfactants, such as poly(ethylene glycol) alkyl ethers (abbreviated as C_yE_x) show a rich phase behavior in aqueous solution, i.e., they form micellar, lamellar, cubic, and so forth phases depending on experimental parameters such as the hydrophobic and hydrophilic chain lengths, temperature, or concentration. The aim of the present study is to determine the nature of the preaggregates, which are inferred to exist before the actual self-assembly process in aqueous solution, and to assess the aptitude to their formation. The target molecules are $C_{12}E_3$, $C_{12}E_4$ and $C_{12}E_5$, surfactants of moderate water solubility. Coarse-grained and all-atom molecular dynamics simulations (NPT/293 K) of two molecules of each species with explicit water in periodic boundary conditions are carried out to estimate the mutual orientation and the interaction between the surfactants in their dimers. The force fields are MARTINI and Amber99, the latter with self-derived parameters for the ether groups. The change in the orientation and distance between the molecules in the dimers are discussed based on different structural parameters. In addition, the interaction between the surfactants is evaluated from quantum chemistry calculations in terms of binding energy for the average structures from the cluster analysis. The solvent–solute interaction is quantified by the mean number of hydrogen bonds formed between them. On the basis of combined analysis, a series of different structures for subsequent study of the possible self-assembly patterns of $C_{12}E_3$, $C_{12}E_4$, and $C_{12}E_5$ is outlined.

	1	2	3	4	5
$C_{12}E_3$	 -1.30	 -2.96	 -2.86	 -0.56	 2.43
$C_{12}E_4$	 -3.21	 -3.41	 -2.17	 -3.07	 0.05
$C_{12}E_5$	 -0.70	 -3.38	 -5.70	 -4.13	 -7.73

INTRODUCTION

Poly(ethylene glycol) alkyl ethers are typical nonionic surfactants with general chemical structure, $H(CH_2)_y(OCH_2CH_2)_xOH$, which is simply denoted by C_yE_x , where y corresponds to the number of carbon atoms in the hydrocarbon tail, and x corresponds to the number of oxyethylene residues in the head. C_yE_x with different numbers of ethylene glycol units and various hydrophobic chain lengths form a chemically stable homologue series, and their compounds are commercially available. These surfactants exhibit high surface activity, and their aqueous solutions show surface tension behavior characteristic for aggregation in a very low-concentration range, namely, from 10^{-7} to 10^{-6} mol·dm $^{-3}$,¹ orders of magnitude below their critical micelle concentration (CMC), which is on the order of 10^{-5} to 10^{-4} mol·dm $^{-3}$.² Beyond the CMC, this class of surfactants forms a variety of neat and mesomorphic phases depending on the chemical composition of the surfactant and on the temperature.^{3–10} The chemical structure also allows tuning of the hydrophilic/hydrophobic balance by varying the number of oxyethylene and methylene units responsible for the solubilization in the respective liquid phase. The CMC value of the various C_yE_x homologues depends on the number of ether oxygens and grows with the increase of this number.²

In diluted aqueous solutions, such surfactants exist mainly in the micellar or in the lamellar phases depending on the

chemical nature and molecular structure of the surface-active species and on the thermodynamic conditions. In pure or mixed solvents, these nonionic surfactants can produce a large variety of self-assembled structures relevant to several fields of application. In the form of emulsions, microemulsions, vesicles, or liposomes, such systems are extensively used in detergency, stabilizing and recovery from pollutants, or as nanotransporters.^{11–13} The propensity of C_yE_x to self-assemble in various shapes and sizes can be used in certain novel materials, e.g., nanoporous structures with controlled dimensions of the pores, for which C_yE_x micelles with different size are used as templates.¹⁴ Therefore, knowledge about the factors governing the existence of the various phases of C_yE_x supramolecular assemblies at the molecular level is valuable.

In this study, the target molecules are $C_{12}E_3$, $C_{12}E_4$, and $C_{12}E_5$. $C_{12}E_3$ is known to form only bilayers in the bulk, while $C_{12}E_4$ and $C_{12}E_5$ are able to self-assemble in cylindrical micelles in solution.¹⁵

Recently, molecular dynamics (MD)¹⁶ and Monte Carlo¹⁷ simulations have been successfully applied to study poly(ethylene glycol) chains in water or nonionic surfactants in an assortment of phases (at the air/water interface^{18,19} and in

Received: December 14, 2011

Revised: March 3, 2012

Published: March 26, 2012



lamellar²⁰ or micellar phases^{21–23}). All these studies accentuate the fact that the conformation of the surfactant head (the E_x -fragment) depends on its hydration,²⁴ and the *gauche* helix is preferred to the *trans* form, in agreement with experimental observations of similar systems.^{25,26}

A foregoing investigation on $C_{12}E_5$ ²⁷ provided evidence that its micellization proceeds in three stages: (i) fast aggregation in clusters containing a small number of monomers, (ii) growth of the aggregates due to incorporation of single monomers or to fusion of small micelles, and finally (iii) attainment of micelles of persistently stable size. Therefore, the characterization of the primary clusters, the so-called preaggregates observed in the first stage of the self-organization, will shed light on the driving forces of this process. Moreover, there is also indirect experimental evidence for the formation of preaggregates at very low surfactant concentrations,¹ but their microscopic nature cannot be assessed experimentally. Thus, the current study aims to determine the C_yE_x preaggregates type assumed to exist in aqueous solution prior to formation of the real micelles, and to provide a quantitative estimate of the aggregation affinity.

METHODS AND MODELS

The focus of this study is the nonionic surfactants $C_{12}E_3$, $C_{12}E_4$, and $C_{12}E_5$, differing only in the length of the hydrophilic head (Figure 1). The variation of the number of ethylene glycol

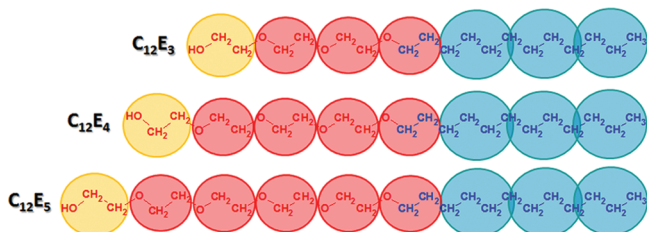


Figure 1. Chemical formulas and 4–1 scheme of coarse-graining of the nonionic surfactants of alkyl poly(ethylene glycol) type $C_{12}E_3$, $C_{12}E_4$, and $C_{12}E_5$.

moieties allows a fine control on the hydrophobic/hydrophilic balance in the molecule and may result in dissimilar propensity to the formation of supramolecular aggregates.

The investigation comprises two stages. To the end of performing an exhaustive conformational space search and sampling of diverse alignments and conformations of the molecules under study, the first stage consists in coarse-grained

MD (CGMD) simulations of two identical $C_{12}E_x$ molecules placed randomly at the beginning in a simulation box with explicit water solvent in periodic boundary conditions (PBCs). The utilized CG model of the surfactants is shown in Figure 1. The CGMD is carried out with the MARTINI force field.²⁸ The latter is chosen because it reproduces well empirically measured characteristics describing the behavior of various surfactants both in the bulk and at the air/water interface, such as density, diffusion rate, area per surfactant head, surface tension, etc.^{29–32} Three of the molecular fragments developed within MARTINI³³ are employed for the description of the dodecyl oligo(ethylene glycol)s: C1 for the hydrocarbon tail (blue), SP2 for the hydroxyl group (yellow), and SNa for the ethylene glycol residues (red). Coarse-grained water³¹ is used as solvent. The simulation is performed in NPT ensemble, maintaining the pressure at 1 bar and the temperature at 293 K by a Berendsen barostat and thermostat.³⁴ The short-range nonbonding and electrostatic interactions are evaluated at a cutoff of 12 Å, introducing a switch function at 10 Å; the long-range electrostatic contributions are assessed by particle mesh Ewald (PME).³⁵ The time step is 10 fs, and the production part of the CGMD trajectory is 1 μs.

For more detailed information of the dimers conformations and their interaction with the water molecules by means of hydrogen bonds, as well as for elucidation of the stabilizing role of H-bonding, all-atom (AA) MD simulations are carried out next. For this purpose, cluster analysis is applied to the CGMD trajectory and structures differing in the mutual orientation of the two $C_{12}E_x$ molecules within a dimer are selected as initial ones for the AA simulations. The criterion for the formation of a dimer is distance less than 1.5 nm between the centers of mass (COMs) of the two molecules. The chosen CG dimers are converted into AA ones and for each of them, a separate MD simulation is run. All initial structures used are presented in Figures S1–S3 (Supporting Information). Their number grows with head size due to enhanced conformational freedom. A few analogous geometries are also included in order to obtain better statistics and to check the reproducibility of the MD results. The simulations are run again in NPT ensemble at 293 K and 1 bar of pressure, the time step is 2 fs, and the production part of the AAMD trajectory is 10 ns. The O–H bonds in the water molecules are constrained with SETTLE,³⁶ and the LINCS algorithm³⁷ is used for the rest of the hydrogen-containing bonds. The remaining simulation parameters repeat those of the CG approach. The force field is AMBER99*, i.e., AMBER95³⁸ appended with our own parameters for the ether fragments.³⁹ The water model is TIP4P.⁴⁰

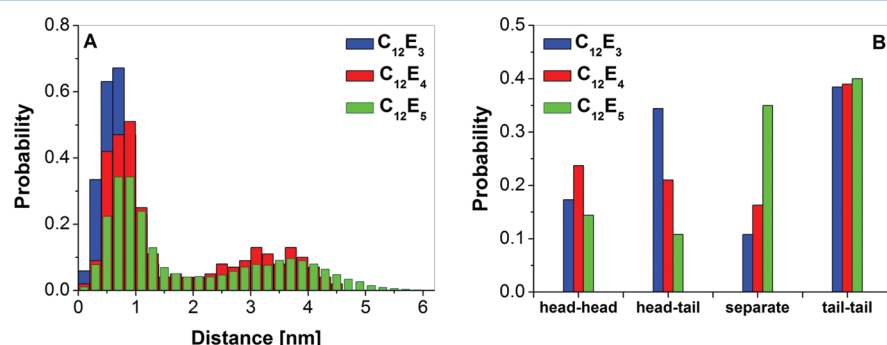


Figure 2. (A) Probability distribution of the distance between the COM of the surfactants, and (B) summarized clustering of the CG structures obtained from the MD simulation, based on the mutual orientation of the molecules in the dimers of the nonionic surfactants $C_{12}E_x$.

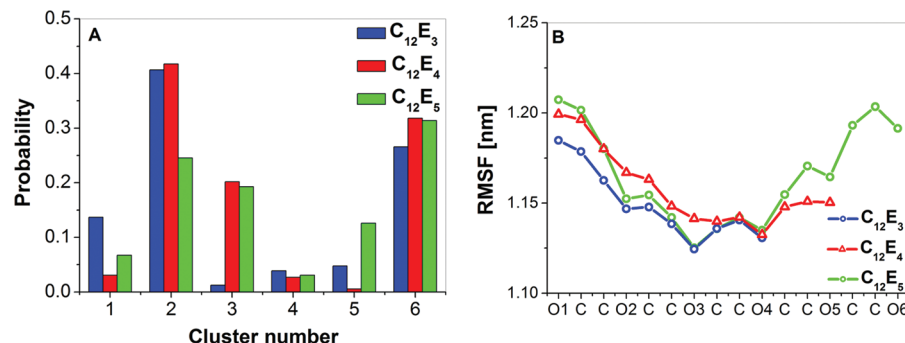


Figure 3. (A) Clustering of AAMD structures based on the distance and mutual orientation of the $C_{12}E_x$ dimers, and (B) RMSF for each non-hydrogen atom in the head of $C_{12}E_x$ (numbering starts from the OH-group oxygen).

Finally, using the MP2 method with the 6-31G* basis set, the binding energies (with basis set superposition error (BSSE) correction) for the average structure of the most populated dimer conformations obtained from the cluster analysis of the AAMD trajectories are calculated for quantification of the dimerization aptitude of $C_{12}E_x$ and determination of the preferred alignment of the monomers.

All MD simulations are performed with GROMACS 4.0;⁴¹ for part of the results, methods of analysis from the package Amber 8⁴² are utilized. Frames for the AAMD statistical analysis are collected at intervals of 1 ps. VMD⁴³ is employed for visualization of the trajectories. The quantum chemical calculations are made with Gaussian 09.⁴⁴

RESULTS AND DISCUSSION

CGMD Simulations. The CGMD trajectory is analyzed, and structures in which the molecules are at a distance on the order of a single surfactant dimension (~ 1.5 nm) or less are selected. This threshold is chosen to ensure interaction between the two molecules in the dimer, and the particular value is substantiated by the analysis of the probability distribution of the distance between the COMs of the molecules presented in Figure 2A: the most populated peak for the three surfactants is in the range 0.4–1.5 nm. Figure 2A also reveals a tendency toward increasing of the intermolecular distance in the dimers and of the number of single monomers in the solution with extension of the surfactant head. Additional confirmation of the enhanced solubility⁴⁵ and reduced affinity for dimerization of $C_{12}E_4$ and $C_{12}E_5$ provide the results from the cluster analysis of the CGMD frames based on the mutual orientation of the two molecules in the dimer shown in Figure 2B. Structures in which the molecules are spaced at larger distances belong to the group “separate”, and the probability for this type of orientation is comparatively large, especially for $C_{12}E_5$. However, in all three cases, the number of structures in this group remains lower than the sum of those classified in the other groups, thus proving the considerable dimerization affinity of the three surfactants.

The plot in Figure 2B demonstrates that the dominating orientation is tail–tail, irrespective of the head size. The next highly populated group is that with head–tail orientation, its probability decreasing in the order $C_{12}E_3$, $C_{12}E_4$, $C_{12}E_5$. The probability of the fourth group, head–head, does not show any definite correlation with the head size. The growing population of “separate” structures upon extension of the hydrophilic head is always at the expense of depopulation of the latter two groups, indicating that mainly short heads aggregate effectively.

AAMD Simulations. The AAMD results disclose two alternatives: some dimers have retained their initial configuration, and others have assumed different orientation of the monomers. Among those conserving their orientation (within the statistical confidence) are mainly members of the tail–tail group, the most populated group after the CG clustering. It can be concluded that transitions from the other types of orientation to the more stable tail–tail one are frequent, which is expected because of the hydrophobic character of the tails. These structures should be the most abundant and predominant as preaggregates.

The most populated orientations obtained from the AAMD cluster analysis are shown in Figure 3A, and the average structures are presented in Table 1. Six groups can be outlined.

Table 1. Average Structures Obtained from the Cluster Analysis of the AAMD Trajectories (Figure 3A) of the $C_{12}E_x$ Dimers and the Corresponding MP2/6-31G* Binding Energies (kcal/mol)

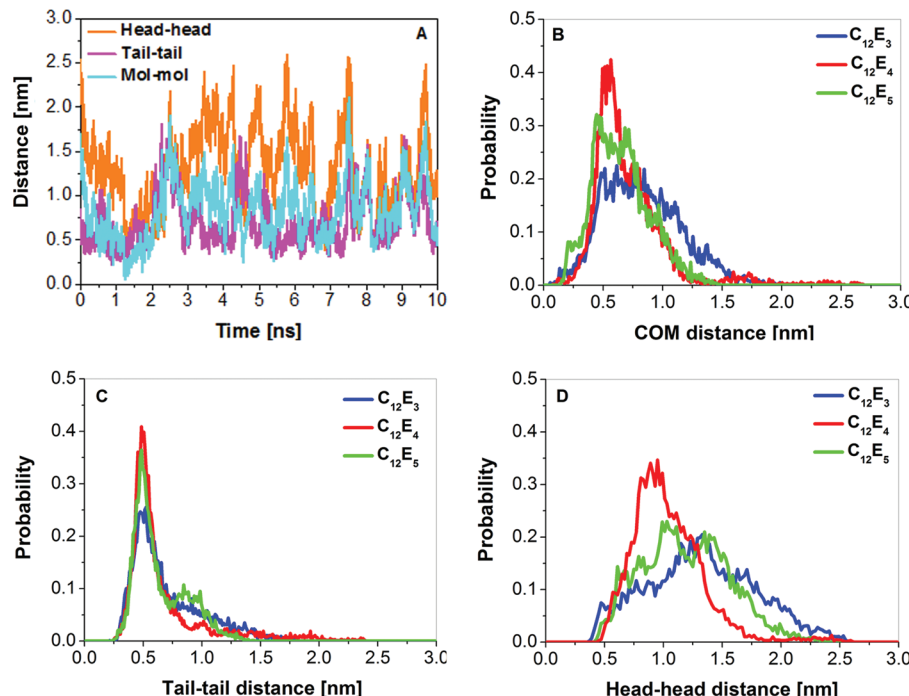
	1	2	3	4	5
$C_{12}E_3$	 -1.30	 -2.96	 -2.86	 -0.56	 -2.43
$C_{12}E_4$	 -3.21	 -3.41	 -2.17	 -3.07	 0.05
$C_{12}E_5$	 -0.70	 -3.38	 -5.70	 -4.13	 -7.73

Group 6 contains the structures in which the molecules are at distances larger than 1.5 nm. The probability for separation of the monomers is relatively large, similar to that in the CG simulations, but the disproportion between the three kinds of surfactants is smaller, which may be due to the different time scale. $C_{12}E_5$ and $C_{12}E_4$ feature approximately equal detachment probability, whereas $C_{12}E_3$ exhibits a diminished number of unbound monomers owing to its lower solubility in water compared to the other two surfactants.⁴⁵

The dimer structure and monomer orientation in the other five groups manifest some trends analogous to the CG simulation. In a nutshell, the preferred orientation is tail–tail, corresponding to groups 1, 2, and 3. In group 4, the alignment is head–tail, which is modestly populated for all three surfactants, as illustrated in Figure 3A. Group 5 comprises the head–head orientations and is negligibly populated for $C_{12}E_4$.

Table 2. Average Number of Hydrogen Bonds between the Ether Oxygen of the Head and the Water Molecules

group number	1	2	3	4	5
$C_{12}E_3$	7.80 ± 1.38	7.98 ± 1.38	7.54 ± 1.43	7.27 ± 2.47	7.63 ± 1.43
$C_{12}E_4$	9.09 ± 1.57	9.82 ± 1.60	9.34 ± 1.55	8.57 ± 1.56	8.69 ± 1.55
$C_{12}E_5$	10.91 ± 1.69	10.99 ± 1.70	10.69 ± 2.79	9.35 ± 1.70	10.37 ± 1.72

Figure 4. (A) Time evolution (from a simulation of $C_{12}E_3$, where 85% of the structures belong to group 1), and probability distributions of the (B) molecule₁–molecule₂, (C) tail₁–tail₂, and (D) head₁–head₂ distances in the group 1 structures of the three surfactants.

The AAMD cluster analysis prompts the general conclusion that more favorable alignments for $C_{12}E_3$ are the one with close tails and distant heads or that with approximately equidistant molecular fragments. For $C_{12}E_4$, most populated are the dimers with proximate tails and remote heads, and only in the case of $C_{12}E_5$ in addition to the latter structures do the ones with both neighboring heads and tails (cluster 5) have sizable presence.

The finding that tails pack more readily than heads is in agreement with the amplified flexibility of the heads due to the *gauche* effect in the ethylene glycol residues, which grows with head size and remains obscured in the coarse-grained models. In contrast, the tails retain the *trans* conformation in the majority of structures and fluctuate less during the simulation. The root-mean-square fluctuation (RMSF) of each non-hydrogen atom of the head is calculated as a measure of its mobility (Figure 3B). Most flexible is the free end of the head of each surfactant, the mobility decreasing along the chain toward the tail. Enhanced mobility of the atoms linking heads with tails is observed in $C_{12}E_4$ and $C_{12}E_5$ owing to the incidence of folded conformations (see Table 1). Such structures (group 3) are rare in $C_{12}E_3$ and become more frequent with elongation of the head. It is noticeable that the curves for surfactants with an odd number of ethylene glycol residues have similar profiles, which alludes to analogy in the mobility mode of the atoms in the heads. The curve for $C_{12}E_4$ has an intermediate profile closer to that of $C_{12}E_5$.

The trends revealed by the cluster analysis are supported by the values of the binding energy, E_{bind} , of the average dimer structures of each group (Table 1). For all dimers (with one

exception), the binding energy is negative, which confirms the propensity for aggregation of $C_{12}E_x$. However, the E_{bind} values of $C_{12}E_x$ depend both on orientation and head size. It is noteworthy that clusters with close tails and remote heads feature stabilization of about 3 kcal/mol owing to dimerization for all three surfactants. The only positive value of E_{bind} is observed in structures where the interaction involves only small portions of the $C_{12}E_4$ heads. This unfavorable alignment explains the low population probability of group 4 in the cluster analysis of this surfactant. On the other hand, the head–tail interaction becomes more favorable with lengthening of heads, maybe due to the larger number of methylene groups in longer heads. This strengthened attraction between heads and tails in the higher homologues, competitive to the tail–tail interaction, also expedites the more pronounced fluctuations in the heads of $C_{12}E_4$ and $C_{12}E_5$ (Figure 3B). The largest binding energy is that of the average structure of group 5 for $C_{12}E_5$, which is the most compact one and permits simultaneous interaction between all fragments of the two molecules. The substantial population of this group could also be rationalized in terms of this strong intermolecular coupling.

Table 2 contains the averaged number of hydrogen bonds between the water molecules and the oxygen atoms in the heads of the $C_{12}E_3$, $C_{12}E_4$, and $C_{12}E_5$ dimers. It grows with head size and head accessibility. This tendency is somewhat analogous to that of E_{bind} –head size but is more consistent. Although the average values between the separate groups look identical within the standard deviations, they have been proven to be statistically dissimilar by a two-sided *t* test. The H-bond

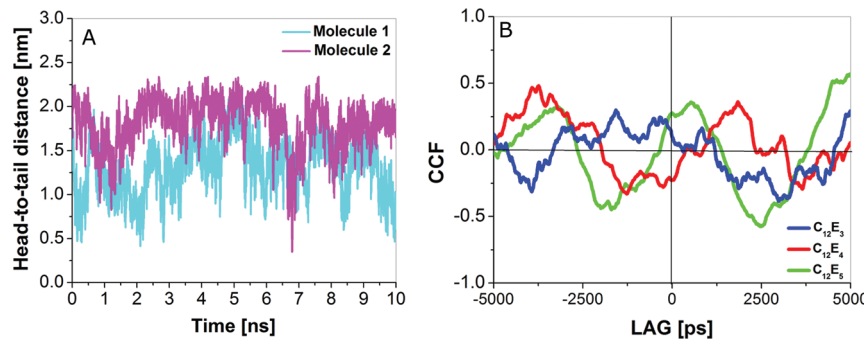


Figure 5. (A) Time evolution of the head-to-tail distance of each molecule in the dimer (from a simulation of C₁₂E₃, where 85% of the structures belong to group 1), and (B) correlation function of this distance for the group 1 structures of the three surfactants.

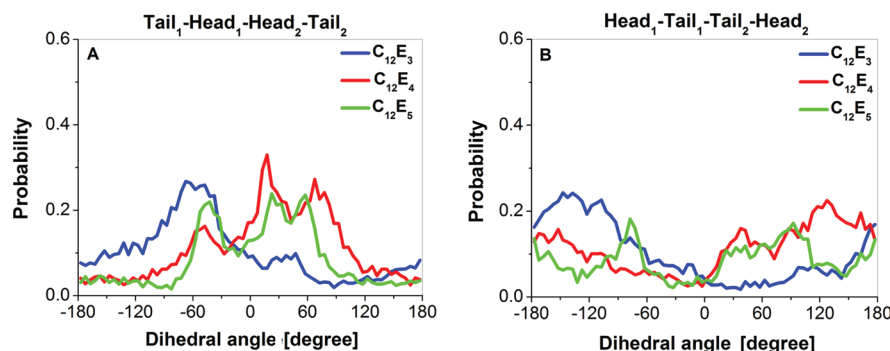


Figure 6. Probability distribution of the dihedral angles (A) tail₁-head₁-head₂-tail₂ and (B) head₁-tail₁-tail₂-head₂ for the group 1 structures of the three surfactants.

formation plays a dual role in aggregation: on the one hand, it stabilizes the aggregates by providing a friendly environment for the heads; on the other, it facilitates the separation of the monomers, especially for larger heads, the energy gain of complete solvation being more important than E_{bind} . Head exposure to the solvent is the second key factor determining the number of H-bonds. The most populated group 2 (quite stable also in terms of E_{bind}) forms the largest number of hydrogen bonds, since tails are close together and heads are sufficiently apart to benefit the full access to solvent. Groups 1 and 3 have slightly lower numbers of H-bonds due to the growing compactness of one of the monomers, reducing its contact surface with water molecules. In the least populated group 4, the head of each monomer is screened by the entirely hydrophobic tail of the other, thus obstructing interactions with the solvent, hence, the lowest number of H-bonds. The species in group 5 bind effectively only in the head-head + tail-tail configuration where the hydrophobic coupling results in higher values of E_{bind} . This again diminishes to a certain extent the solvent access, thus reducing their stabilization due to solvation. Particularly, the representative structure of C₁₂E₄, where the possibility for hydrophobic interaction is negligible, has a positive value of E_{bind} and its occurrence is mediated exclusively by H-bonding. Bearing in mind that the population probability of the five groups of dimers is roughly proportional to the estimated number of hydrogen bonds, it can be concluded that H-bonding plays a significant role for the formation and stabilization of preaggregates.

The time evolution and the probability distributions of certain parameters such as distances between the separate fragments of the molecules (between the COMs of the heads, the tails, and the entire molecules) and conformation (head-to-

tail distance of an individual monomer) are analyzed for dimer groups 1–5. For a quantitative assessment of the presence/absence of correlation between the monomer conformations in the dimer, the cross-correlation function (CCF) of the head-to-tail distances of the two molecules is calculated using the *xcor* module of the program suite TISEAN.⁴⁶ The mutual orientation of the monomers in the dimers is estimated by means of the distributions of two dihedrals between the COMs of the fragments: tail₁-head₁-head₂-tail₂ and head₁-tail₁-tail₂-head₂.

Group 1. Characteristic for the dimers in group 1 is that one of the monomers is extended, while the other one is folded around the first. This group is found for all three surfactants with minor variations of structure and orientation.

In Figure 4B–D are presented the probability distributions of the distances molecule₁–molecule₂, tail₁–tail₂ and head₁–head₂. A narrow peak is observed for the tail–tail distance with a maximum at approximately the same distance (~0.5 nm) for each of the surfactant systems and a broader curve (covering the interval 0.5–2.5 nm) for the head–head separation. Here the odd-residue heads behave analogously, while the head–head distance distribution in C₁₂E₄ is noticeably narrower. Overall, the C₁₂E₃ molecules are the most mobile in the dimers. The time evolution of the molecule–molecule distances (Figure 4A) shows that the surfactants stay close during the entire simulation following the fluctuations of the head–head distance, which is a general tendency in group 1.

The time evolution of the head-to-tail distance of each molecule in the dimer (termed occasionally molecular “length”) shown in Figure 5A reveals a predominant more folded conformation of one of the monomers (in cyan) and preference to *trans* conformation of the other (magenta); neither of them

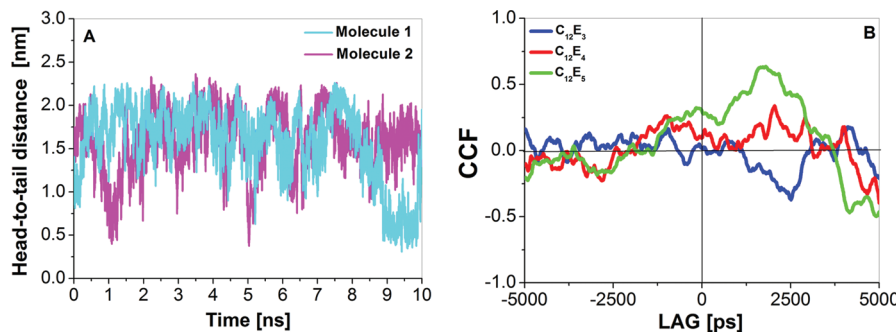


Figure 7. (A) Time evolution of the head-to-tail distance of each molecule in the dimer (from a simulation of C₁₂E₅, where 90% of the structures belong to group 2) and (B) correlation function of these distances for the group 2 structures of the three surfactants.

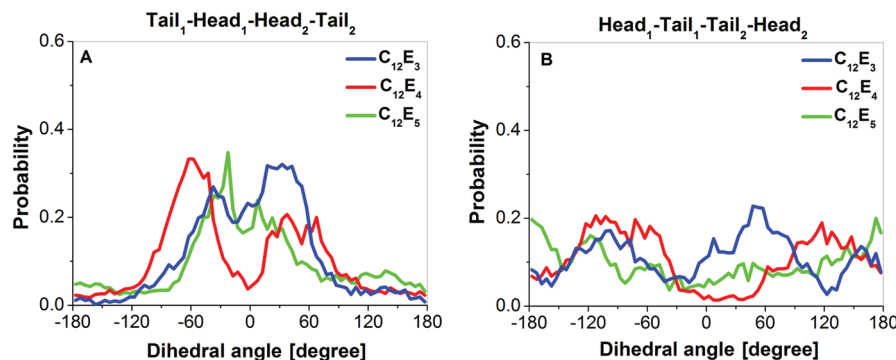


Figure 8. Probability distribution of the dihedral angles (A) tail₁-head₁-head₂-tail₂ and (B) head₁-tail₁-tail₂-head₂ for the group 2 structures of the three surfactants.

reaches the value 2.54 nm corresponding to the fully stretched C₁₂E₃ chain. In the course of the simulation, there are regions where the “lengths” of the two molecules fluctuate in an anticorrelated manner (the one shrinks when the other stretches) and regions where they change synchronously. Which factor then governs the monomer conformation within the dimer: the interaction with the other surfactant, or the individual MD?

The answer can be extracted from the CCF of the two head-to-tail distances plotted in Figure 5B. The witnessed trend is that the correlation grows with head-size. For all three surfactants, CCF oscillates between positive and negative values, i.e., from correlated to anticorrelated change of the head-to-tail distances. Nevertheless, for C₁₂E₃ the extreme values are quite low, indicating rather independent mobility of the monomers in the dimers. CCF for C₁₂E₄ encompasses larger ranges of more substantial correlation, particularly in the negative lags, indicating that one of the molecules plays a leading role for the conformational variations of the monomers in the dimer. The C₁₂E₅ plot features sizable correlation of the head-to-tail distances of the two molecules in the entire interval of displacements, demonstrating that their motion is synchronous throughout the time period. The monitored molecular behavior in the course of the MD simulation supports this finding. The nodes of CCF allow determination of the correlation lengths, which can be related to the characteristic lifetime (τ) of a certain molecular orientation in the dimers. For the group 1 structures τ is in the range 1.2–2.0 ns.

The values of the dihedrals tail₁-head₁-head₂-tail₂ (Figure 6A) are typically between -120° and 120°, the interval contracting upon head enlargement. The same effect is observed for the other dihedral (Figure 6B); ill-shaped maxima

can be discerned around -90° and 90° for the C₁₂E₅ structures, shifted to -120° and 120° (or larger) for the C₁₂E₃ and C₁₂E₄ dimers. This indicates that in the majority of dimers, the identical fragments of the monomers are apart.

Group 2. This is the most populated group encompassing structures with tail-tail orientation, the displacement of the tails being essentially identical for the three surfactants (Figure S4C of the Supporting Information). Another characteristic of this group is the enhanced head flexibility, illustrated in Figure S4D by the head-head distance distribution. An exception are the C₁₂E₅ structures displaying different conduct caused by the high mobility of the oxygen linking the surfactant head and tail (Figure 3B), which permits folding of the monomers resulting in shorter head-head distances (see Table 1).

The distances between the molecules and their fragments (Figures S4B-D) vary in comparatively narrow limits, the tails being systematically closer than the heads. As in group 1, the time evolution of distances is dominated by the heads (Figure S4A) shaping the profile of the molecule₁-molecule₂ distance. The narrower distributions of the group 2 structures are an indication of a more constant orientation of the monomers, stabilized by the largest number of H-bonds (Table 2), and agrees with the tighter binding compared to group 1 (Table 1).

The evolution of the molecular “length” of each monomer (Figure 7A) shows that most of the time both molecules are semiextended with prevailing parallel “length” fluctuations along the trajectory. The fully extended chain of C₁₂E₅ is 3.29 nm long. More compact conformations are witnessed for short periods: ~1 ns for molecule₁ and in the range 9–10 ns for molecule₂. On the whole, the conformation of molecule₂ is quite steady during the simulation.

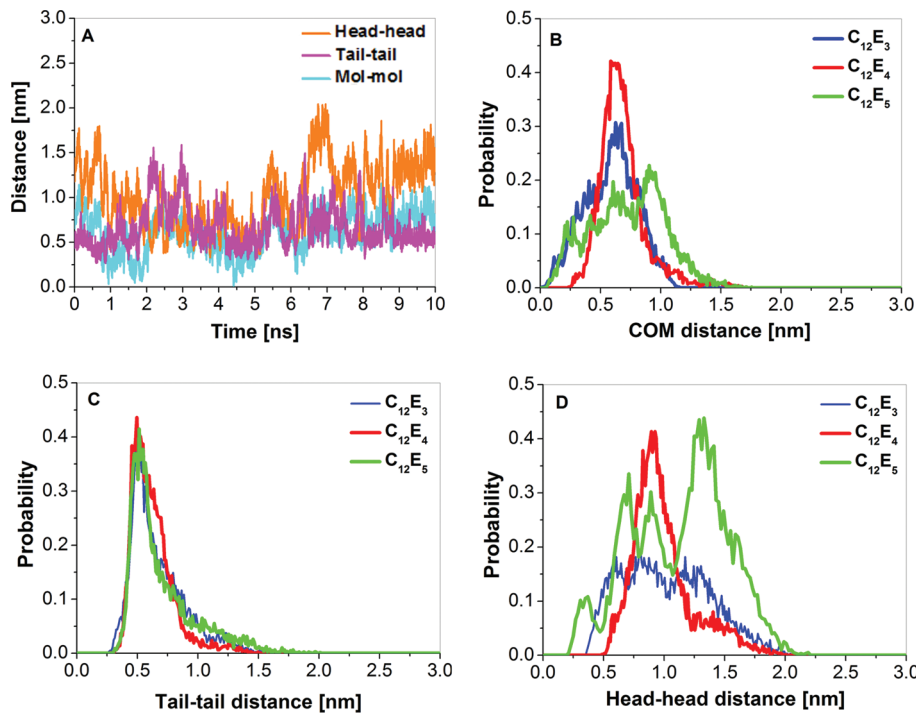


Figure 9. (A) Time evolution (from a simulation of C₁₂E₃, where 79% of the structures belong to group 3), and probability distributions of the (B) molecule₁–molecule₂, (C) tail₁–tail₂, and (D) head₁–head₂ distances in the group 3 structures of the three surfactants.

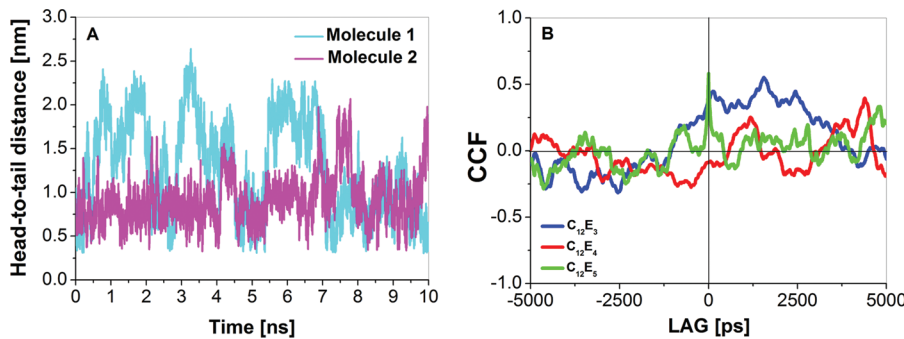


Figure 10. (A) Time evolution of the head-to-tail distance of each molecule in the dimer (from a simulation of C₁₂E₃, where 85% of the structures belong to group 3), and (B) correlation function of these distances for the group 3 structures of the three surfactants.

The correlation between the head-to-tail distances is insignificant for C₁₂E₃ and C₁₂E₄, whereas substantial positive correlation is found for C₁₂E₅ (Figure 7B). The correlation amplification upon head extension is analogous to group 1, but the correlation character of the head-to-tail-distances for the C₁₂E₅ dimers in group 2 is different. Evident correlation is observed only for positive displacements, meaning that one of the monomers plays a leading role for the conformational behavior within the dimer. This is in keeping with the parallel fluctuations of molecular “lengths” during the simulation and relates well with the more compact distance distributions of the fragments. Moreover, the characteristic lifetimes of the molecular orientation in the dimers of this group are longer ($\tau \sim 3.75$ ns), i.e., the structures in this group are more steadfast.

The most probable values of the tail₁–head₁–head₂–tail₂ dihedral are about $\pm 30^\circ$ for C₁₂E₃ and C₁₂E₅, shifted to $\pm 60^\circ$ for C₁₂E₄, but all angles between -120° and 120° are populated for the three surfactants (Figure 8A). Although the probability maxima are at dissimilar values of the angle for the different

surfactants, the profiles of the curves are analogous. The bimodal distribution of the two dihedrals in C₁₂E₄ is noteworthy, while C₁₂E₅ demonstrates preference to 0° values of the tail₁–head₁–head₂–tail₂ angle. Overall, the preferred angles are in the range -75° to 75° , indicating that instead of taking antiparallel alignment, the tails close a small angle. The population plot of the head₁–tail₁–tail₂–head₂ angle (Figure 8B) exhibits no distinct maxima but most preferred are the values about $\pm 180^\circ$, $\pm 120^\circ$, and $\pm 60^\circ$, corresponding to a certain periodicity in the occurrence of this angle. The presence of multiple maxima and the fact that almost the full spectrum of angles has nonzero probability confirms the intense head mobility of the three surfactants. Since the “length” of the molecules is relatively steady (Figure 7A), this implies that the heads move in a plane orthogonal to the one defined by the tails.

Group 3. This group comprises structures with proximate tails of one very compact and one more stretched surfactant molecule. This hampers the consistent discrimination of the differences among the evolutions of the distances between the

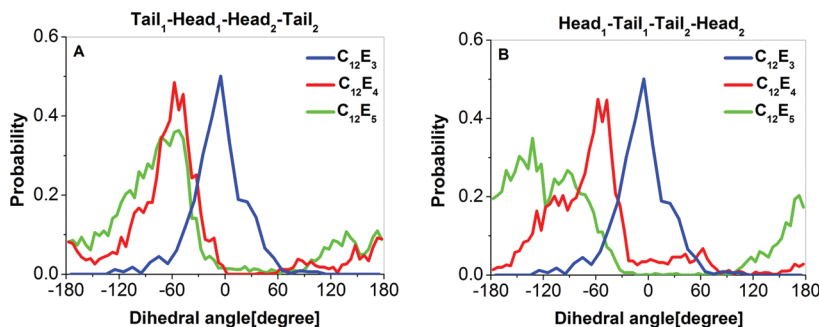


Figure 11. Probability distribution of the dihedral angles (A) tail₁–head₁–head₂–tail₂ and (B) head₁–tail₁–tail₂–head₂ for the group 3 structures of the three surfactants.

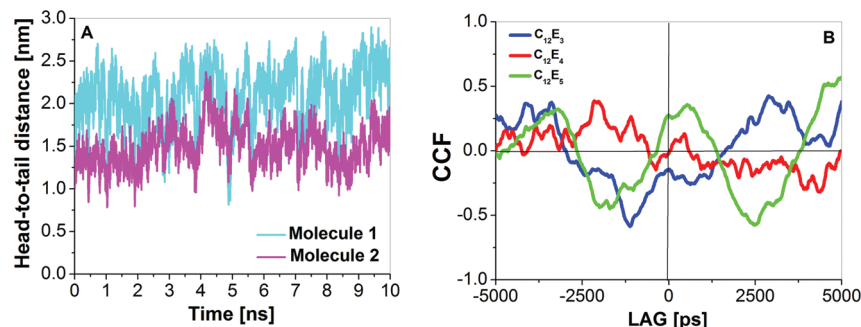


Figure 12. (A) Time evolution of the head-to-tail distance of each molecule in the dimer (from a simulation of C₁₂E₄, where 80% of the structures belong to group 4, and (B) correlation function of these distances for the group 4 structures of the three surfactants.

molecules, their identical fragments and the angles they form. The dimers in this group also display flexible heads and closely coupled tails, similar to group 2. Both parallel and antiparallel alignment of the monomers is witnessed. Unlike the previous two groups, the molecule₁–molecule₂ distance profile is governed by that between the tails. Most of the time the COMs of the monomers and those of their tails are very close in space (Figure 9A–C), while the head–head distances fluctuate more actively. However, group 3 features the most concise head–head distance probability distribution (Figure 9D) so far, with well-defined maxima for C₁₂E₄ and C₁₂E₅. The profiles of the latter distribution differ from surfactant to surfactant. Detailed analysis discloses that apart from the alignment described above the surfactants with odd-residue heads assume a variety of additional orientations in which the monomers are corrugated to a different extent. Among them are structures with antiparallel alignment of the molecules corresponding to large head–head distances. The incidence of such structures is comparatively low for C₁₂E₄, which explains its narrower distribution of this distance.

With respect to molecular conformations, it is visible that one of the molecules stays folded most of the time, and the “length” of the other one varies widely from 0.5 to 2.0 nm (Figure 10A). The correlation between head size and molecular “length” in this group contrasts that in the preceding two: here the correlation decreases with head extension (Figure 10B). The dimers of C₁₂E₃ exhibit substantial correlation in the positive lag section, subsiding progressively in C₁₂E₄ and C₁₂E₅. This shows that in the C₁₂E₃ dimers one of the monomers defines the molecular conformation of the other, while the monomers of the larger homologues fluctuate independently. This finding can not be related to the highest binding energy of C₁₂E₅ in this group, proving that dimers dynamics is governed by more factors than just the energy of intermolecular

interaction. The lack of correlation for the larger species implies that their dynamics depends on the interaction of the fragments within one monomer or on the coupling to the solvent instead.

Typical for the structures in this group are the similar profiles of probability distributions of the two dihedrals (Figure 11). The most populated values for the tail₁–head₁–head₂–tail₂ dihedral are in the range from −120° to 0° with maxima at −60° for the dimers of C₁₂E₄ and C₁₂E₅. The probability distribution curve for the head₁–tail₁–tail₂–head₂ dihedral looks analogous for C₁₂E₄, while the low broad peak of C₁₂E₅ is shifted toward −180°. In C₁₂E₃ the most populated values of both angles are in the same interval: between −60° and 60° with maxima at 0°. This indicates a tendency toward divergence of the heads upon increasing of their size while the tails remain relatively parallel.

Group 4. This group includes dimers with head–tail orientation. This organization is well represented in the set of initial structures, but after the AAMD simulation, the probability of this type of coupling is modest for all three surfactants.

Due to the antiparallel alignment of the two monomers in group 4, the distances between the identical fragments are expected to be larger, which is supported by their probability distribution plots in Figure S5B–D of the Supporting Information. Even the hitherto identical curves of the tail₁–tail₂ distance for the three surfactants show two peaks for this group, one of them corresponding to separated monomers. The profile of the time evolution of the distance between the molecules in the dimer follows that of the heads as in groups 1 and 2 (Figure S5A).

The evolution of the molecular “length” (Figure 12A) testifies that both monomers are stretched throughout the simulation, their head-to-tail distances fluctuating in both

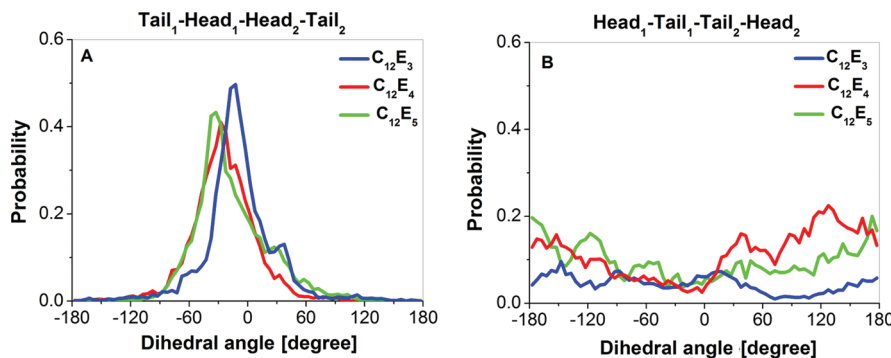


Figure 13. Probability distribution of the dihedral angles (A) tail₁–head₁–head₂–tail₂ and (B) head₁–tail₁–tail₂–head₂ for the group 4 structures of the three surfactants.

parallel and antiparallel manners. The CCF plots in Figure 12B reveal the same picture. For the surfactants with odd-residue heads, the correlation is strong, of both positive and negative sign. Most pronounced is the head-to-tail correlation in C₁₂E₅. None of the monomers plays a leading role in the conformational variation – this fact, as well as the characteristic conformation lifetimes (τ in the range 1.2–2.0 ns, a bit longer in C₁₂E₃), are the analogies between groups 4 and 1.

The structures in this group demonstrate a well-defined peak in the tail₁–head₁–head₂–tail₂ angle distribution at about 0° (Figure 13A) which shifts to larger values upon head enlargement. This is evidenced by highly preferred essentially parallel orientation of the tails. The dihedral head₁–tail₁–tail₂–head₂ takes values from −180° to 180° with almost equal probability.

Group 5. This group consists of strictures with head–head orientation. This type of organization is rare. Moreover, the molecules undergo marked conformational changes and the outline of similarities between the groups formed by each surfactant is an intricate task. The assignment of structures to group 5 is based only on the head–head orientation. A detailed analysis of the obtained results for this group is presented in the Supporting Information on pages S6–S8.

CONCLUSIONS

The main objective of this study is the investigation of the aggregation affinity and characterization of the geometry of dimers of amphiphilic alkyl ethers of oligo(ethylene glycol)s in aqueous solution. Conformationally diverse initial structures are sampled after cluster analysis of CGMD and subject to AAMD simulations. The trajectories are analyzed with respect to conformation of the monomers, their mutual orientation in the dimers, the energy of binding, and the solvent effect. The structures are classified in six groups based on the first two factors. All simulations are in explicit solvent.

After the CGMD, dimers with predominating tail–tail orientation prevail, in correspondence with the hydrophobic character of the tails and their drive to evade the polar solvent. This tendency persists after the AAMD, with preference to *trans* conformation in most of the tails. In contrast, the heads are very flexible due to the *gauche* effect in the ethylene glycol residues. The evolution of the distance between the molecules follows the oscillations of the head–head distance, indicating that the heads are the driving force for the MD, most probably because of their favorable interaction with the surrounding water molecules. The dihedral angles between the COMs of the fragments (tail₁–head₁–head₂–tail₂ and head₁–tail₁–tail₂–

head₂) can be used as parameters determining the monomer orientation in the dimer because they have specific profiles in each group obtained after clustering. Conformation changes of the surfactant molecules are observed in all groups, and all-*trans* conformations are almost missing. It is noteworthy that in 2/3 of the structures, one of the monomers retains a relatively unaffected conformation, i.e., acts as an “anchor”, while the other monomer undergoes more prominent changes. Both synchronous and independent conformational modifications are witnessed as evidence of the finding that the orientation of monomers in the dimer is dynamic, but there is a tendency toward the establishment of a relatively steady global configuration. The dimerization affinity is also illustrated by the fact that, even after short periods of sizable separation, the monomers recouple and stay close together for considerable time periods. This is supported by the negative values of the binding energy, obtained at various molecular alignments.

Head size has no significant influence on the number and type of the groups based on the dimer configuration. Overall, the relationships for the three surfactants are analogous. The increase of the number of C–O–C moieties results in enhanced flexibility and mobility of the heads. Substantial correlation of the monomer conformations within the dimers is noticed mainly for C₁₂E₅. The lifetime of a certain orientation in a dimer does not exceed 1–2 ns, which shows that the C₁₂E_x dimers are fairly dynamic formations.

The synergy between the binding energy of the monomers in the dimers and the number of hydrogen bonds formed between the dimers and the solvent explains the pronounced preference to dimers with tail–tail orientation (groups 1–3), leaving room for other geometries stabilized by one of these two factors. Since the affinity for dimerization is expressed best in the structures with tail–tail orientation, which are appropriately organized for further aggregation, they can be attributed to the preaggregates existing in diluted solutions.

Finally, it should be emphasized that the sorting in groups is provisional, aiming to systematize the statistical analysis, because in each simulation much more than one kind of structure occurs; only the percentage varies. This shows that the transition from one pattern of orientation to another is feasible, i.e., it could be concluded that the dimers are excessively dynamic structures. However, the simulations unequivocally reveal that the vast majority of dimers are in tail–tail configuration during most of the time, irrespective of their particular mutual alignment, which is favorable for the eventual formation of large supramolecular aggregates.

■ ASSOCIATED CONTENT

§ Supporting Information

The following data are provided as Supporting Information: **Figure S1:** Initial structures obtained from CGMD used for AAMD simulations of C₁₂E₃. **Figure S2:** Initial structures obtained from CGMD used for AAMD simulations of C₁₂E₄. **Figure S3:** Initial structures obtained from CGMD used for AAMD simulations of C₁₂E₅. **Figure S4:** Time evolution and probability distributions of the molecule₁–molecule₂, tail₁–tail₂, and head₁–head₂ distances in the group 2 structures of the three surfactants. **Figure S5:** Time evolution and probability distributions of the molecule₁–molecule₂, tail₁–tail₂, and head₁–head₂ distances in the group 4 structures of the three surfactants. **Figure S6:** Time evolution and probability distributions of the molecule₁–molecule₂, tail₁–tail₂, and head₁–head₂ distances in the group 5 structures of the three surfactants. **Figure S7:** Correlation function of the head-to-tail distances of the separate molecules in the dimer for the group 5 structures of the three surfactants. **Figure S8:** Probability distribution of the tail₁–head₁–head₂–tail₂ and head₁–tail₁–tail₂–head₂ dihedral angles for the group 5 structures of the three surfactants. This material is available free of charge via the Internet at <http://pubs.acs.org>.

■ AUTHOR INFORMATION

Corresponding Author

*E-mail: tadjer@chem.uni-sofia.bg; tel.: +359-2-8161374; Fax: +359-2-962-54-38.

Notes

The authors declare no competing financial interest.

■ ACKNOWLEDGMENTS

This work is funded by Projects DO-02-256/2008, DCVP-02-2/2009 and DO-02-136/2008 of NSF-BG, and supported by the FP7 project BeyondEverest.

■ REFERENCES

- (1) Arabadzhieva, D.; Tchoukov, P.; Mileva, E.; Miller, R.; Soklev, B. *Ukr. J. Phys.* **2011**, *56*, 2071–2076.
- (2) Rosen, M. J.; Cohen, A. W.; Dahanayake, M.; Hua, X. Y. *J. Phys. Chem.* **1982**, *86*, 541–545.
- (3) Kunieda, H.; Nakamura, K.; Davis, H. T.; Evans, D. F. *Langmuir* **1991**, *7*, 1915–1919.
- (4) Mitchell, D. J.; Tiddy, G. J. T.; Waring, L.; Bostock, T.; McDonald, M. P. *J. Chem. Soc., Faraday Trans. 1* **1983**, *79*, 975–1000.
- (5) Olsson, U.; Wurz, U.; Strey, R. *J. Phys. Chem.* **1993**, *97*, 4535–4539.
- (6) Olsson, U.; Shinoda, K. B. *J. Phys. Chem.* **1986**, *90*, 4083–4088.
- (7) Vasilescu, M.; Caragheorgheopol, A.; Almgren, M.; Brown, W. A., J.; Johannsson, R. *Langmuir* **1995**, *11*, 2893–2898.
- (8) Shimobouji, T.; Matsuoka, H.; Ise, N.; Oikawa, H. *Phys. Rev. A* **1989**, *39*, 4125–4131.
- (9) Zana, R.; Weill, C. *J. Phys. Lett.* **1985**, *46*, 953–960.
- (10) Tiddy, G. J. T. *Phys. Rep.* **1980**, *57*, 2–46.
- (11) Mitchell, D. J.; Tiddy, G. J. T.; Waring, L.; Bostock, T.; McDonald, M. P. *J. Chem. Soc., Faraday Trans. 1* **1983**, *79*, 975–1000.
- (12) Shinoda, K.; Saito, S. *J. Colloid Interface Sci.* **1968**, *30*, 258–263.
- (13) Florin, E.; Kjellander, R.; Eriksson, J. C. *J. Chem. Soc., Faraday Trans. 1* **1984**, *80*, 2889–2910.
- (14) Ryu, J. H.; Park, S.; Kim, B.; Klaikhherd, A.; Russell, T. P.; Thayumanavan, S. *J. Am. Chem. Soc.* **2009**, *131*, 9870–9871.
- (15) Srinivas, G.; Nielsen, S. O.; Moore, P. B.; Klein, M. L. *J. Am. Chem. Soc.* **2006**, *128*, 848–853.
- (16) Tasaki, K. *J. Am. Chem. Soc.* **1996**, *118*, 8459–8469.
- (17) Engkvist, O.; Karlstrom, G. *J. Phys. Chem. B* **1997**, *101*, 1631–1633.
- (18) Kuhn, H.; Rehage, H. *J. Phys. Chem. B* **1999**, *103*, 8493–8501.
- (19) Chanda, J.; Bandyopadhyay, S. *J. Chem. Theory Comput.* **2005**, *1*, 963–971.
- (20) Bandyopadhyay, S.; Tarek, M.; Lynch, M. L.; Klein, M. L. *Langmuir* **2000**, *16*, 942–946.
- (21) Sterpone, F.; Briganti, G.; Pierleoni, C. *Langmuir* **2001**, *17*, 5103–5110.
- (22) Sterpone, F.; Pierleoni, C.; Briganti, G.; Marchi, M. *Langmuir* **2004**, *20*, 4311–4314.
- (23) Garde, S.; Yang, L.; Dordick, J. S.; Paulaitis, M. E. *Mol. Phys.* **2002**, *100*, 2299–2306.
- (24) Yoshida, H.; Takikawa, K.; Kaneko, I.; Matsuura, H. *J. Mol. Struct.* **1994**, *311*, 205–210.
- (25) Viti, V.; Indovina, P. L.; Podo, F.; Radics, L.; Némethy, G. *Mol. Phys.* **1974**, *27*, 541–559.
- (26) Matsuura, H. F. *K. J. Mol. Struct.* **1985**, *126*, 251–260.
- (27) Velinova, M.; Sengupta, D.; Tadjer, A.; Marrink, S.-J. *Langmuir* **2011**, *27*, 14071–14077.
- (28) Marrink, S. -J.; de Vries, A. H.; Mark, A. E. *J. Phys. Chem. B* **2004**, *108*, 750–760.
- (29) Jalili, S.; Akhavana, M. *Colloids Surf., A* **2009**, *352*, 99–102.
- (30) Lee, H.; Pastor, R. W. *J. Phys. Chem. B* **2011**, *115*, 7830–7837.
- (31) Marrink, S. J.; Risselada, H. J.; Yefimov, S.; Tieleman, D. P.; Vries, A. H. d. *J. Phys. Chem. B* **2007**, *111*, 7812–7824.
- (32) Sangwai, V. A.; Sureshkumar, S. *Langmuir* **2011**, *27*, 6628–6638.
- (33) Lee, H.; de Vries, A. H.; Marrink, S. -J.; Pastor, R. W. *J. Phys. Chem. B* **2009**, *113*, 13186–13194.
- (34) Berendsen, H. J. C.; Postma, J. P. M.; DiNola, A.; Haak, J. R. *J. Chem. Phys.* **1984**, *81*, 3684–3691.
- (35) Essmann, U.; Perera, L.; Berkowitz, M. L.; Darden, T.; Lee, H.; Pedersen, L. G. *J. Chem. Phys.* **1995**, *103*, 8577–8594.
- (36) Miyamoto, S.; Kollman, P. A. *J. Comput. Chem.* **1992**, *13*, 952–962.
- (37) Hess, B.; Bekker, H.; Berendsen, H. J. C.; Fraaije, J. G. E. M. *J. Comput. Chem.* **1997**, *18*, 1463–1472.
- (38) Cornell, W. D.; Cieplak, P.; Bayly, C. I.; Gould, I. R.; Merz, K. M.; Ferguson, D. M.; Spellmeyer, D. C.; Fox, T.; Caldwell, J. W.; Kollman, P. A. *J. Am. Chem. Soc.* **1995**, *117*, 5179–5197.
- (39) Velinova, M.; Tsoneva, Y.; Shushkov, Ph.; Ivanova, A.; Tadjer, A. In *Advances in the Theory of Quantum Systems in Chemistry*; Hoggan, P. E., Brändas, E. J., Maruani, J., Piecuch, P., Delgado-Barrio, G., Eds.; Progress in Theoretical Chemistry and Physics Series; Springer Science+Business Media B.V.: New York, 2011, Vol. 22; Chapter 26, pp 461–480, DOI 10.1007/978-94-007-2076-326.
- (40) Jorgensen, W. L.; Madura, J. D. *Mol. Phys.* **1985**, *56*, 1381–1392.
- (41) van der Spoel, D.; Lindahl, E.; Hess, B.; Groenhof, G.; Mark, A. E.; Berendsen, H. J. C. *J. Comput. Chem.* **2005**, *26*, 1701–1718.
- (42) Case, D. A.; Darden, T. A.; Cheatham, T. E., III; Simmerling, C. L.; Wang, J.; Duke, R. E.; Luo, R.; Merz, K. M.; Wang, B.; Pearlman, D. A. et al. *AMBER 8*, University of California: San Francisco, CA, 2004.
- (43) Humphrey, W.; Dalke, A.; Schulten, K. *J. Mol. Graphics* **1996**, *14*, 33–38.
- (44) Frisch, M. J.; Trucks, G. W.; Schlegel, H. B.; Scuseria, G. E.; Robb, M. A.; Cheeseman, J. R.; Scalmani, G.; Barone, V.; Mennucci, B.; Petersson, G. A. et al. *Gaussian 09*; Gaussian, Inc.: Wallingford, CT, 2009.
- (45) Jonstroemer, M.; Sjoerberg, M.; Waernheim, T. *J. Phys. Chem.* **1990**, *94*, 7549–7555.
- (46) Hegger, R.; Kantz, H.; Schreiber, T. *Chaos* **1999**, *9*, 413–435.